In-depth analysis of coal chemical structural properties response to flue gas saturation: perspective on long-term CO_2 sequestration

Major Mabuza*

Department of Chemical Engineering Technology,
University of Johannesburg,
P.O. Box 17011, Doornfontein,
Johannesburg 2088, South Africa
Email: majorm@uj.ac.za
*Corresponding author

Kasturie Premlall

Department of Chemical, Metallurgical and Materials Engineering,
Tshwane University of Technology,
Private Bag X680, Pretoria 0001, South Africa
Email: premlallk@tut.ac.za

Mandlenkosi G.R. Mahlobo

Department of Chemical and Materials Engineering,
University of South Africa,
P.O. Box 392, Florida 1709, South Africa
Email: mahlomg@unisa.ac.za

Abstract: A comprehensive study on the chemical structural properties of coals after flue gas exposure is significant to consider long-term carbon dioxide (CO_2) sequestration in deep and unmineable coal reservoirs. Two South African coals were exposed to a five-component synthetic flue gas typical of a coal-fired power plant for 90 days at 9.0 MPa pressure and 60°C temperature. Advanced characterisation techniques were used, including carbon-13 solid-state nuclear magnetic resonance spectroscopy (^{13}C ^{ss}NMR), universal attenuated total reflectance-Fourier transform infrared (UATR-FTIR), field emission gun scanning electron microscopy with energy dispersive X-ray spectroscopy (FEG SEM-EDX), and wide-angle X-ray diffraction (WXRD) to capture the chemical structural changes. The results show weakened functional groups of –OH, out-of-plane aromatic C–H, aliphatic C–O, C–C, and C–H. There is structural deformation in the crystalline diameter and inter-layer spacing that is sorption-induced owing to the flue gas saturation, and the coals oxygen functionalities revealed notable changes. [Received: October 22, 2023; Accepted: July 7, 2024]

Keywords: advanced characterisation; chemical structural properties; CO_2 sequestration; flue gas; unmineable coal seams.

Reference to this paper should be made as follows: Mabuza, M., Premlall, K. and Mahlobo, M.G.R. (2024) 'In-depth analysis of coal chemical structural properties response to flue gas saturation: perspective on long-term CO_2 sequestration', *Int. J. Oil, Gas and Coal Technology*, Vol. 36, No. 5, pp.1–17.

Biographical notes: Major Mabuza is Senior Lecturer in the Department of Chemical Engineering Technology, University of Johannesburg, South Africa. He holds a DEng in Chemical Engineering from Tshwane University of Technology. His main research interests fall within the fields of chemical and metallurgical engineering, primarily focusing on carbon capture, utilisation and storage (CCUS); metal-organic frameworks (MOFs) for carbon dioxide capture; landfill biogas recovery (process and materials); and recovery of rare earth elements (REEs) from coal fly ash.

Kasturie Premlall is a Lecturer in the Department of Chemical, Metallurgical and Materials Engineering, at Tshwane University of Technology, South Africa. She holds a PhD in Chemical Engineering from University of Witwatersrand. Her main research interests fall within the fields of chemical and metallurgical engineering, primarily focusing on carbon capture, utilisation and storage (CCUS); metal-organic frameworks (MOFs) for carbon dioxide capture; landfill biogas recovery (process and materials); corrosion technology and inhibition techniques; and the recovery of rare earth elements (REEs) from AMD and coal fly ash.

Mandlenkosi G.R. Mahlobo is a Senior Lecturer at the Department of Chemical and Materials Engineering, University of South Africa. He obtained his PhD from the University of Johannesburg in collaboration with the University of La Rochelle. His primary research area entails electrochemical techniques for corrosion of various materials in various applications. His secondary research area includes carbon capture, utilisation and storage (CCUS). His research experience further extends to studies on gasification of biomass for hydrogen production. He also has industrial experience on bio-heap leaching of low-grade copper and gold ores.

1 Introduction

The sequestration of carbon dioxide (CO_2) in geological formations, particularly the unmineable coal seams, is a promising and attractive opportunity to mitigate the effect of global warming as a result of anthropogenic CO_2 greenhouse gas emissions (Ali et al., 2022). This is mainly because coal seams possess a large ratio of surface area to volume, allowing them to offer up to seven times more potential CO_2 storage than other geological reservoirs (Salmachi et al., 2023). Implementing carbon sequestration technology in geological formations requires assurance of long-term stabilisation of the storage site and secure and safe long-term CO_2 storage (Tcvetkov et al., 2019). Due to the complex nature of the coal structure, CO_2 sequestration in unmineable coal reservoirs has proven to be an intricate phenomenon. Few researchers have examined the long-term fate of CO_2 through various CO_2 capture mechanisms in coal seams, its distribution within the coal matrix, and long-term site stabilisation following CO_2 injection (Zhang et al., 2021a). Some of the related studies include those that were recently conducted by Chen et al. (2023), Merey (2022) and Zhang et al. (2021b), and have reported on the fate of

pure supercritical CO_2 injected in unmineable coal seams and the effect on the chemical and structural properties of the coal; even so, their investigations were limited to surface chemistry and textural properties of the coals probed. For instance, the study by Zhang et al. (2021b) found that the Neimark fractal dimension of coals is increased by prolonged CO_2-H_2O exposure, further suggesting increased pore surface roughness and greater complexity in the pore structure, with reduced oxygen functionalities, particularly C–O, C=O, and –COOH.

In the context of directly injecting industrial flue gas in deep and unmineable coal reservoirs, no knowledge has been reported yet in literature on long-term storage and the long-term interactions between flue gas and coal under in-situ pressure and temperature conditions. The concept of direct flue gas injection in unmineable coal seams has predominantly focused on ECMB. Related studies were first reported by Mazumder et al. (2006) in which more investigations by other researchers (Huo et al., 2019; Mazumder et al., 2008; Syed et al., 2013; Talapatra, 2020; Xing et al., 2020) followed; however, all these studies are mainly based on sorption isotherm measurements as well as correlating the data to coal rank, maceral composition, sorption capacity of individual gases, and the use of flue gas for enhanced coalbed methane (ECBM) recovery. Early studies by Mazumder et al. (2006) conducted a study to evaluate the Polish Silesian Basin coal sorption properties using pure CO_2 and a custom flue gas (0.01% CO, 10.9% CO_2, 0.106% SO_2, 3.01% CH_4, 3.0% O_2, and balance N_2) as adsorbates at maximum pressure and temperature of 11 MPa and 80°C, respectively, using the volumetric method. Their study showed that the additional gases only reduce the partial pressure of CO_2 for sorption and do not significantly hinder the CO_2 sorption affinity and behaviour of coal. However, their custom flue gas did not incorporate essential components of a typical industrial flue gas coal-fired power plant, including NOx; also, temperature variations were not considered. Durucan and Shi (2009) and Syed et al. (2013) conducted similar studies using binary gases consisting of CO_2 and N_2, with average molar compositions of 13% and 87%, respectively. Sorption experiments of binary gases are an excellent threshold in upscaling to multi-component gases, but they may not give more insight since they do not represent a close resemblance to a flue gas (Lukhele et al., 2017; Mabuza et al., 2018).

Talapatra (2020) analysed various scenarios for enhancing coalbed methane recovery processes, including injecting flue gas directly into the coal reservoirs. They concluded that this approach is strikingly an appealing alternative in the way of considerably increasing gas production; also, this approach may drive the elimination of the much more expensive CO_2 capture stage, hence offsetting the related costs (Das et al., 2023). however, this would require collectively compressing all the flue gas components, mainly N_2, since it has very weak sorption power on coal with respect to CO_2. In a recent study by Zhou et al. (2023) which focused on the heat-fluid-solid interactions between the flue gas and coal during ECBM, they discovered that the sharp reduction in the coal permeability caused by pure CO_2 injection is significantly prevented when injecting a flue gas. Furthermore, it was found that the flue gas effective extraction zones expand more rapidly with respect to CO_2 and, subsequently, produce more recovery gas. Table 1 summarises key previous studies that have been undertaken on direct flue gas injection in unmineable coal seams in the past decade; the summary includes the locations of the probed coals, coal type, experimental conditions, and the physicochemical properties evaluated. Table 1 further outlines that most of the studies to date focused on pre-sorption

evaluation of the chemical structural properties of the coals, mainly proximate analysis, and petrography, and no post-sorption investigations were conducted.

Table 1 Summary of sorption data reported in literature in comparison to the current study

Location	*Coal type*	*Gas compositions*	*Experimental conditions*	*Physicochemical coal properties evaluated*	*Reference*
Silesia, Poland	Bituminous C	$CO_2/CO/H_2/CH_4/O_2/SO_2/N_2$	80°C, 11 MPa	*Pre-sorption:* petrography *Post-sorption*: no evaluation	Mazumder et al. (2006)
Scotland, UK	Bituminous A	CO_2/N_2	26 °C, 6.89–8.41 MPa	*Pre-sorption:* proximate analysis; petrograph; textual	Syed et al. (2013)
	Bituminous B			*Post-sorption:* no evaluation	
	Bituminous C				
Shaanxi, China	Anthracite A	CO_2/CH_4	28°C, 10 MPa	*Pre-sorption:* proximate analysis; petrography	Yu et al. (2014)
	Anthracite B			*Post-sorption:* no evaluation	
	Bituminous A				
Springlake Colliery, RSA	Anthracite B	CO_2/SO_2	35°C, 9.0 MPa	*Pre-sorption:* proximate analysis; petrograph *Post-sorption:* no evaluation	Lukhele et al. (2017)
Shaanxi, China	Bituminous C	$CO_2/N_2/O_2/CH_4$	20–60°C, 5.0 MPa	*Pre-sorption:* proximate analysis; petrograph; surface chemistry (FTIR) *Post-sorption:* no evaluation	Zheng et al. (2020)
Ermelo, RSA	Bituminous C	$CO_2/N_2/O_2/SO_2/NO_2$	30–60°C, 9.0 MPa	*Pre-sorption:* proximate and ultimate analysis; petrography; surface chemical analysis (UATR-FTIR and ^{13}C ^{ss}NMR); micro-crystallinity and morphology (WXRD and FEG SEM-EDX)	This study
Somkhele, RSA	Anthracite C			*Post-sorption:* same as pre-sorption except for proximate and ultimate analysis	

As such, examining the chemical structural properties is necessary to understand the interaction between flue gas and coal in the context of direct flue gas sequestration in unmineable coal reservoirs. These properties primarily include the coal morphology, crystallinity, and surface chemistry. The parallel view into the alterations in textural properties was recently addressed by Mabuza and Premlall (2023). Therefore, this paper

presents a new viewpoint and results of an in-depth analysis of the long-term effects of coal saturated with flue gas on the chemical structural properties of coals during CO_2 sequestration. The coal samples investigated in this study were extracted from two South African regions:

1 Somkhele coalfields (SKL)

2 Ermelo coalfields (ERL).

The extracted coal samples were exposed to a synthetic industrial flue gas from a typical coal-fired power plant for 90 days, and various advanced analytical characterisation techniques were employed, including UATR-FTIR, ^{13}C ^{ss}NMR, FESEM-EDX, and WXRD.

2 Experimental methods

2.1 Sample collection and preparation

In this study, two coal samples, including ERL and SKL, were collected from the historical central coal mining regions of the South African Karoo basin based on their petrography in terms of maceral composition and rank. The ERL was collected from Ermelo coalfield, and SKL was collected from Somkhele coalfield, as shown in Figure 1. All the received samples were wrapped in zip-lock bags and were stored in refrigerator near ice-point (0°C) after being flushed with inert helium to prevent them from air oxidation (Mastalerz et al., 2009). For the flue gas sorption experiments, the samples were crushed and screened from an average particle size of 50 mm to an average grain size of 2 mm. Sample sizes passing 75 μm screen were used for WXRD, UATR-FTIR, ^{13}C ^{ss}NMR, and standard properties (density, proximate and ultimate analyses), while for petrography and FEG SEM-EDX average grain sizes of 1 mm and 2 mm were used, respectively. The standard and petrography properties of the samples are presented in this study for coal classification and identification purposes; consequently, they were further not examined following exposure to flue gas.

2.2 Flue gas saturation experiments

The flue gas sorption experiment procedure adopted for this study followed that of Mabuza et al. (2018) using a high-pressure volumetric sorption system described by Premlall et al. (2019). The coal samples were saturated with a custom flue gas composed of $CO_2/O_2/N_2/SO_2/NO_2$ with molar fractions of 0.12/0.055/0.82/0.0038/0.0012 at a pressure of 9.0 MPa and temperature of 60°C for 90 days. These temperature and pressure conditions are typical of a coal reservoir depth greater than 800 m, as profiled by Zhang (2008), which is ideal for gas storage since the fluid is supercritical due to the significant increase in temperature and pressure (Raza et al., 2019).

Figure 1 South African map showing various coalfields (see online version for colours)

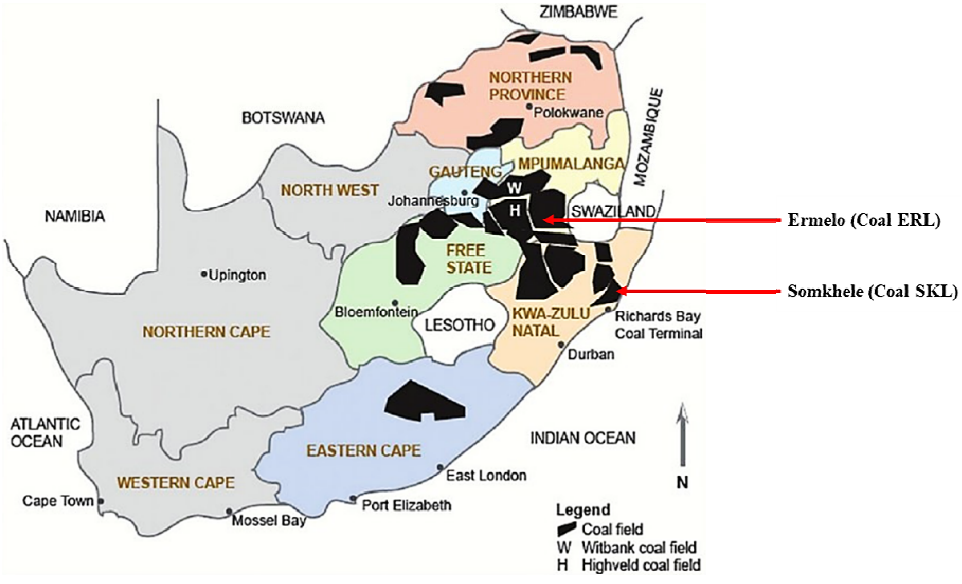

Source: Pinetown et al. (2007) reproduced with permission of Elsevier

3 Results and discussion

3.1 Density, proximate, ultimate, and petrography

The standard properties of the coal matrices in Table 2 include the density, proximate and ultimate analyses, and petrography. Sample ERL and SKL recorded densities of 1.72 g/cm^3 and 1.84 g/cm^3, respectively. The volatile matter in sample ERL is 49.8 wt%, and that of sample SKL is 7.6 wt%. Both the samples yielded a similar ash content ranging from 17.3 to 17.9 wt%; however, with distinct fixed carbon of 27.8 and 74.1 wt% for sample ERL and SKL, respectively. The inherent moisture content is low for both samples, yielding 4.5% for ERL and 1.0 for SKL; similarly, through the ultimate analysis data, the total sulphur recorded for sample ERL is 0.6 wt% while 0.9 wt% was recorded for sample SKL, with comparable nitrogen concentrations of 1.9 wt%.

The petrography data reveals that the maceral group mainly comprised of vitrinite and inertinite groups with some liptinite and mineral compositions. The vitrinite group is dominant in sample SKL (84 vol%), indicating the predominance of organic input from terrestrial xylem, cells, and phloem tissues in higher plant vascular tissues. Sample ERL is inertinite-rich (74.2 vol%), resulting from the gradual oxidation of organic matter of the terrestrial woody plant material. The traces of liptinite (3.3%) in sample ERL stem from the bacteria and algal precursors from the lacustrine environment. The mineral matter (4.5–9.8 vol%) for both samples is composed mainly of quartz, suggesting a depositional of detrital minerals due to low-hydrogen index (HI), as shown in the ultimate analysis data. The vitrinite random reflectance (Ro) recorded a mean of 0.64 and 2.24 vol% for samples ERL and SKL, respectively, signifying that sample ERL is a medium-rank bituminous C coal with sample SKL being high-rank anthracite C coal.

Table 2 Density, proximate, ultimate, and petrography analyses of the coal samples

Analytical method	*Sample*		*ISO method*
	ERL	*SKL*	
Density (g/cm^3)[a]	1.72	1.84	-
Proximate analysis (wt%)[b]			
Volatile matter	49.8	7.6	562:2010
Ash	17.9	17.3	1171:2010
Moisture	4.5	1.0	11722:2013
Fixed carbon	27.8	74.1	By difference
Ultimate analysis (wt%)[c]			
Carbon	75.1	82.0	17247:2013
Hydrogen	4.6	3.1	17247:2013
Nitrogen	1.9	1.9	17247:2013
Oxygen	17.8	12.1	17247:2013
Sulphur*	0.6	0.9	19579:2006
Petrographic analysis			
RoV%	0.64 (0.097)**	2.24 (0.434)**	7404:2009
Rank	Medium rank C	High rank C	11760:2018
Type	Bituminous C	Anthracite C	11760:2018
Maceral analysis (vol%)[d]			
Total vitrinite (TV)	12.8	84.0	11760:2018
Total inertinite (TI)	74.2	11.5	11760:2018
Total liptinite (TL)	3.3	0	11760:2018
Total mineral matter (TMM)	9.8	4.5	602:2015
Total reactive macerals (TRM)	25.6	84.0	By summation

Notes: [a]as received, [b]air dried basis, [c]dry ash-free basis, [d]including mineral matter,
RoV = mean vitrinite random reflectance, **standard deviation, *total sulphur,
TRM = TL + TV + inertodetrinite + reactive semifusinite.

3.2 Chemical-structural properties

3.2.1 Surface chemical analysis (UATR-FTIR and ^{13}C ^{ss}NMR)

Figure 2 displays the untreated and flue gas-saturated samples ERL and SKL's UATR-FTIR spectra. Following the flue gas exposure, the peaks corresponding to the two samples were identified and observed to change marginally and, in some regions, significantly (highlighted with an orange oval shape). This suggests that as the flue gas exposure was prolonged for both samples, their chemical structures were also affected. After flue gas treatment, most of the peaks' IR absorbance did not change significantly from their original spectra, and no new peaks emerged. However, there have been changes to the peaks' percentage transmittance.

Figure 2 UATR-FTIR spectra for, (a) ERL (b) SKL (see online version for colours)

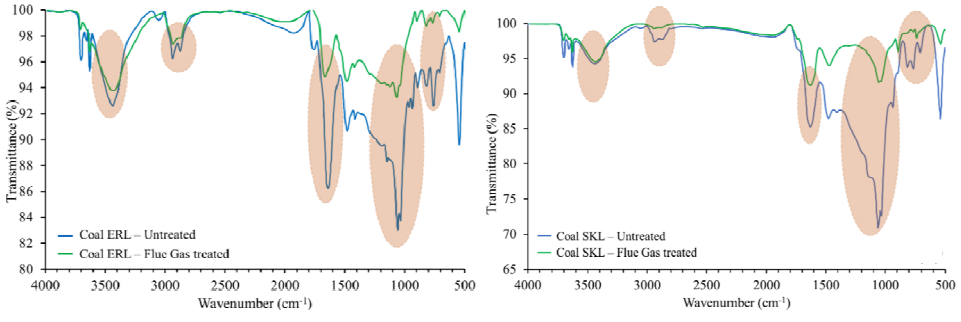

(a) (b)

Table 3 Coals structural parameters determined by the ^{13}C ^{ss}NMR

Carbon assignment (wt%)	*Integral region*	*ERL*		*SKL*	
		Untreated	*FG treated*	*Untreated*	*FG treated*
Total aromatic carbons, f_a	135–90	0.87	0.88	0.91	0.95
Total aliphatic carbons, f_{al}	60–0	0.13	0.12	0.09	0.05
Aliphatic carbons bonded to oxygen, f_{al}^{O}	90–60	0.022	0.038	0.021	0.027
Carbons bonded to carbonyls, f_a^{CO}	200–165	0.07	0.07	0.02	0.05
Carbons bonded to phenolics, f_a^{P}	165–150	0.10	0.12	0.05	0.04
Alkylated aromatic carbons, f_a^{S}	150–135	0.16	0.17	0.15	0.13
Non-protonated carbons in aromatic region, f_a^{N}	–	0.64	0.64	0.73	0.71
Protonated carbons in aromatic region, f_a^{H}	–	0.17	0.18	0.16	0.23
Bridgehead carbons in aromatic region, f_a^{B}	–	0.38	0.33	0.53	0.52
Non-protonated carbons and methyl groups, f_{al}^{N*}	–	0.05	0.02	0.05	0.05
Aliphatic CH and CH_2, f_{al}^{H}	–	0.08	0.11	0.03	0.03

After flue gas saturation, the broad region of the UATR-FTIR spectrum, 3,600–3,100 cm^{-1}, attributed to –OH stretching vibrations, responded differently for samples ERL and SKL. As a result of the high inherent moisture content (4.5%), the intensity of this region remained high and wide for the inertinite-rich sample ERL. Over a prolonged flue gas exposure period, the intensity of this peak gradually decreased. This was caused by the gradual effect of vaporisation of moisture at 60°C over time (Liang et al., 2023), which

yielded an occurrence of dihydroxylation and reduction in the hydroxyl group of the samples. After prolonged flue gas exposure, the broad region intensity for vitrinite-rich sample SKL remained low and wide, indicating the presence of the –OH group due to the low inherent moisture content (1.0%). In contrast to sample ERL, this region was unchanged for sample SKL over the same flue gas saturation period.

There is no IR absorbance in the C–H stretching vibrations region, 3,100–3,000 cm^{-1}, after flue gas treatment for the two samples, particularly for sample ERL. This suggests that there was additional weakening in this region caused by flue gas saturation; this is alluded to an increase in the degree of condensation of coal aromatic nuclei, resulting in the samples being highly substituted (Wu and Zhang, 2019). There are no apparent changes in the aliphatic C=O and –COOH stretching vibrations region, 1,650 cm^{-1}, which is proportionally related to the fraction of carbons bonded to the carbonyls – see ^{13}C ^{ss}NMR results in Table 3; which was also unchanged by the flue gas saturation, especially for sample ERL. The small incremental IR change observed for sample SKL in this region results from the reduced fraction of carbon bonded to the carbonyls due to flue gas saturation.

There was no excessive coalification for the two samples caused by the saturated flue gas; this emerges from the unchanged IR absorption in the aromatic stretching vibrations representing C=C in the region, 1,680–1,500 cm^{-1}. The two samples show a weakened IR absorbance in the –OH bending vibrations, and aliphatic skeletal C–O, C–C stretching, 1,280–1,000 cm^{-1}, which is systematically related to skeletal C–C and C–O stretching vibrations in the phenolic and phenoxy structures of the coals. This observation stems from the reduced phenols concentration – see ^{13}C ^{ss}NMR data in Table 3; this may also be due to the inherent moisture gradually vaporising, consequently decreasing the –OH group (Qin et al., 2010). The small and multiple peaks assigned to the out-of-plane aromatic C–H bending vibrations in the region 900–700 cm^{-1} reveal a sharp decrease in the IR absorbance, suggesting a substantial reduction in the substituted –CH–CH chains (Li et al., 2015; Shao et al., 2019) for the two samples.

The quantitative carbon-13 cross-polarisation magic angle spinning {^{13}C (1H) CP-MAS} is indicated in Figure 3 together with the dipolar-dephasing magic angel spinning (DD-MAS) nuclear magnetic resonance (NMR) spectra for the two samples, with the signal to noise ratio remaining low for the entire spectra range. The integral ranges 60–0, 90–60, 150–90, and 250–200 ppm represent the SSB2, aliphatic regions, aromatic region, and SSB1, respectively, which comparatively show no alterations caused by the induced flue gas saturation since they were all detected within similar frequency ranges. However, sample SKL shows a high-intensity peak for SSB2, which may be interpreted as the magical-angle spinning (MAS) rate being lower than the frequency range of the aromatic carbons' chemical shift anisotropy (CSA) (Xu et al., 2019).

Notably, in Figure 3, the peak intensity of the aromatic region got marginally narrowed for the samples due to prolonged flue gas exposure, which may explain the aromaticity variations as presented in Table 3 and, subsequently, affecting the aliphaticity of the coals. Although there may not be a definitive elucidation for this phenomenon, it is attributable to the heterogeneous nature of the coals (Xu et al., 2021).

The structural parameter of the ^{13}C ^{ss}NMR reveals that there were no significant alterations in the oxygen-containing functionalities (f_{al}^{O}, f_{a}^{CO}, f_{a}^{P}) of the coals, except for the aliphatic carbons bonded to oxygen, f_{al}^{O}, which essentially increased by 42% and

22% for samples ERL and SKL, respectively. This is due to oxygen in the flue gas and partially substituting within the aliphatic chains to form stronger bonds of C–O and COO (Baysal et al., 2016). There were negligible changes in other functionalities, including non-protonated carbons in the aromatic region, f_a^N, and alkylated aromatic carbons, f_a^S.

Figure 3 CP-MAS ^{13}C (1H) with DD-MAS NMR spectra for, (a) ERL (b) SKL showing the integration ranges, including the spinning side bands (SSB1-SSB2) (see online version for colours)

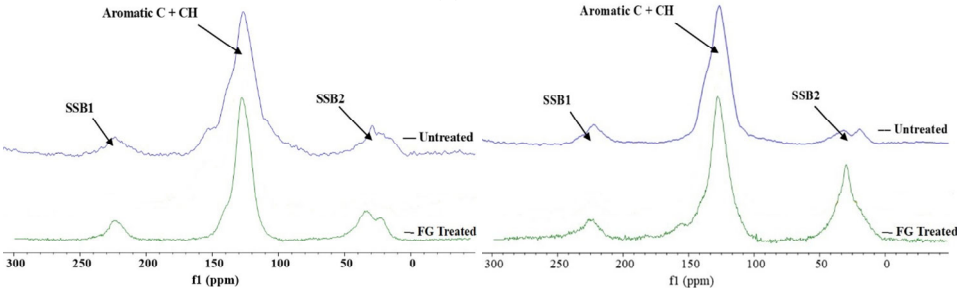

(a) (b)

3.2.2 Micro-crystallinity and morphology (WXRD and FEG SEM-EDX)

The diffractograms are presented in Figures 4(a) and 4(b) for samples ERL and SKL. Each diffractogram shows patterns corresponding to the untreated and flue gas-saturated coal samples. In both ERL and SKL samples, the patterns of the diffractograms corresponding to the untreated and flue gas-treated coal samples exhibited similar peaks and, in some instances, appeared to be superimposed, which indicated the presence of the same crystalline phases on both coal samples. However, the observed peaks in both patterns of untreated and flue gas-treated coal samples showed different intensities, with the flue gas-treated patterns exhibiting significantly larger intensities than those of untreated patterns. This observation implied that flue gas exposure induced significant changes on the surface of the coal samples. Moreover, the sample SKL diffractogram [Figure 4(b)] revealed new peaks after flue gas exposure, implying new crystalline phases on the coal surface. These peaks are observed at approximately 22°, 34°, 43° and 62°. This well outlined the effects of flue gas exposure on the microstructural properties of the coal. The (002) peak increased for the two samples but retained the same peak position. The parameter changes mentioned above indicate a weakened microcrystalline structure of the coal matrix. High-pressure fluids, especially supercritical CO_2, induce swelling in the coal matrix. In this case, the flue gas served as a plasticiser, which expanded the free volume network of the macromolecular glassy-like coal, subsequently enabling coal matrix macromolecular structural rearrangements. The parameter changes mentioned above indicate the weakened microcrystalline structure of the coal matrix. High-pressure fluids, especially supercritical CO_2, induce swelling in the coal matrix. In this case, the flue gas served as a plasticiser, which expanded the free volume network of the macromolecular glassy-like coal, subsequently enabling coal matrix macromolecular structural rearrangements (Du et al., 2018).

Figure 4 WXRD patterns of the coals, (a) ERL (b) SKL (see online version for colours)

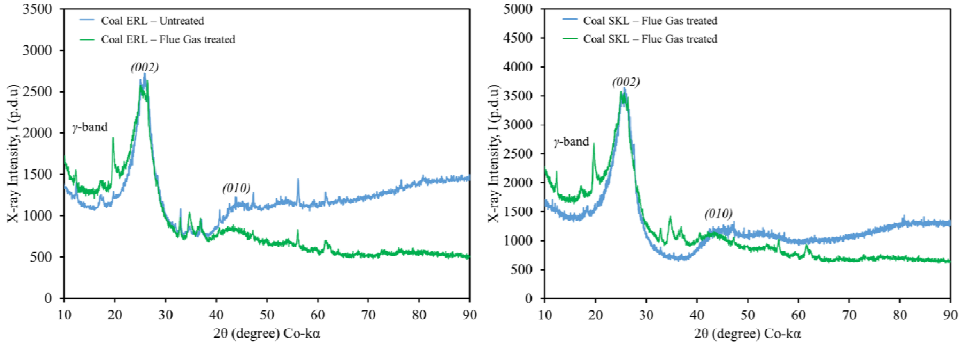

(a) (b)

The high-intensity background shows that after flue gas saturation, the two coal samples still contain amorphous crystalline carbons, being that neither enhanced nor significant spontaneous combustion occurred in the system. The peaks (002) and (010) around 26° and 43° result from these carbons, and these amorphous crystalline carbons occur in the form of graphite-like structure. The retention of the asymmetric γ-band on the left of the (002) band suggests that the two samples have saturated aliphatic side chains. Beyond the (010) band, there are narrow and small peaks; this means that there is a presence of pyrite (FeS_2) and anorthite ($CaAl_2Si_2O_8$) even after flue gas saturation. This occurrence is complementary to the EDX results in Table 5, showing pyrite, quartz, and kaolinite mineralogical occurrences after flue gas exposure.

Table 4 WXRD structural properties and parameters of samples ERL and SKL

Sample	*ERL*		*SKL*	
	Untreated	*FG treated*	*Untreated*	*FG treated*
X'Pert Highscore Plus software derived structural parameters extracted from the WXRD spectra				
Wavelength – λ (Å)	1.51	1.51	1.51	1.51
2θ (°)	26.40	26.68	26.57	27.12
β_{002} – FWHM at 002 band	0.90	0.97	0.14	0.2115
β_{10} – FWHM at 10 band	0.63	0.44	0.12	0.146
Scherrer's constant – K_c at 002 band (–)	0.89	0.89	0.89	0.89
Scherrer's constant – K_a at 10 band (–)	1.84	1.84	1.84	1.84
Structural properties evaluated from Bragg's and Scherrer's laws				
Inter-layer spacing – d_{002} (Å)	1.27	1.08	1.14	0.88
Crystalline height – L_c (Å)	1.84	1.93	12.46	12.13
Crystalline diameter – L_a (Å)	5.44	8.70	30.06	36.33
Aromatic layers per carbon crystalline – N_{ave} (–)	2.45	2.79	11.89	14.74
Aromaticity, f_a (–)	0.84	0.86	0.87	0.92

The WXRD structural properties and parameters for the two samples are presented in Table 4. The crystalline diameter, L_a, and the inter-layer spacing, d_{002}, of the coals appear to have been altered by prolonged exposure to the flue gas. The decrease in the inter-layer spacing was recorded to be 15% and 22.8% for samples ERL and SKL, respectively, relative to untreated coals; this effect causes the inter-layer spacing matrices to collapse. Sample ERL crystalline diameter increased by 37.5%, while that of sample SKL by 17.3%. The alterations in these microcrystalline properties of the coals indirectly validate the coal matrix swell effect due to flue gas induced high-pressure strain, as discussed earlier in this section, which is a result of the effective incorporation of flue gas molecules within the macro- and micromolecular structure of the crystalline carbons (Schaeperkoetter et al., 2019).

Table 5 Mineralogical elemental analysis of samples ERL and SKL

	ERL		*SKL*		
	Untreated	*FG treated*	*Untreated*	*FG treated*	
Element	wt%	wt%	wt%	wt%	Mineral occurrence
C	65.79	58.7	80.68	66.94	graphite
O	14.56	18.19	12.20	15.71	–
Al	2.20	4.1	1.43	2.64	Kaolinite
Si	7.06	7.11	3.79	5.60	Kaolinite/quartz
P	10.40	8.6	0	7.70	Apatite
S	0	3.3	1.90	1.41	Gypsum/pyrite
Total	*100*	*100*	*100*	*100*	

Figure 5 FEG SEM micrographs of sample ERL, (a) untreated (b) flue gas-treated (see online version for colours)

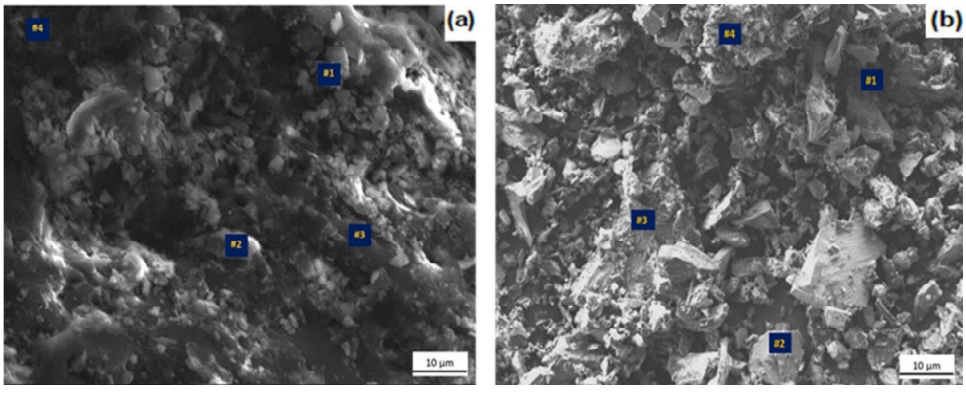

The coal surfaces appear ununiform from the FEG SEM micrographs shown in Figures 5 and 6 for samples ERL and SKL, respectively. This was probable since coal is naturally heterogeneous; hence, the coal surface morphology was expected not to experience any alterations because of flue gas exposure. As a result, the coals maintained their uneven and erratic surfaces with crystals of unidentified shapes – see Figures 5(b) and 6(b). Furthermore, the mineralogical elemental data acquired through EDX (see Table 5) show an emergence of minor mineral impurities, which include P (apatite), S (gypsum), Al

(kaolinite), and Si (quartz). This suggests that the coals experienced some extent of mineralisation during the 90-day period. This is superficially a common phenomenon since Reddy et al. (2011) observed similar behaviour during their experimental study on the mineralisation of flue gas (CO_2, SO_2, NOx) using coal fly ash, in which there was a formation of gypsum ($CaSO_4 \cdot 2H_2O$) due to the presence of SO_2 in the flue gas stream.

Figure 6 FEG SEM micrographs of sample SKL, (a) untreated (b) flue gas-treated (see online version for colours)

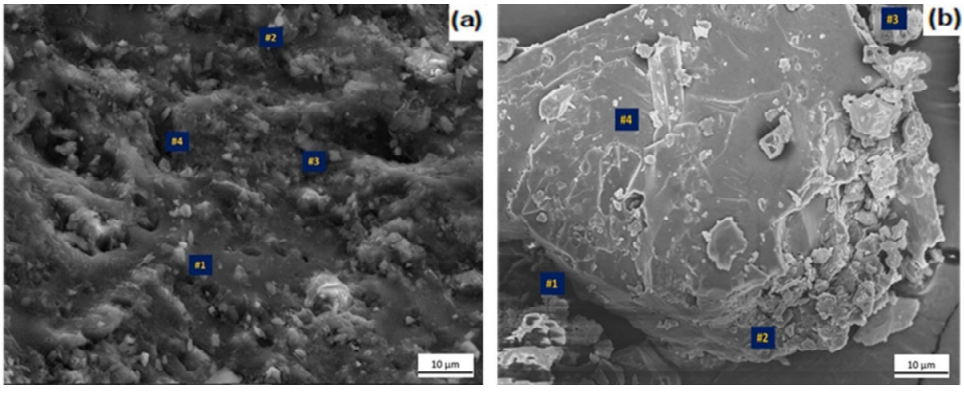

As illustrated in this study, the chemical-structural changes in the coals after gas exposure are not strong enough to be easily understood by FEG-SEM-EDX alone. However, a distinct distinction is made when the FEG SEM-EDX analysis is combined with the WXRD, UATR-FTIR, and ^{13}C ^{ss}NMR analyses. Due to this experience, some researchers (Cheng et al., 2017; Wang et al., 2023; Zhang et al., 2021a) did consider the FESEM-EDX concept in their studies. Then again, most of their attention was mainly on pure CO_2 exposure on coals. Since flue gas saturation on coals rather than pure CO_2 is the focus of this study, it was necessary to investigate any potential chemical-structural changes to the coals using FESEM-EDX analysis in conjunction with the UATR-FTIR, WXRD, and ^{13}C ^{ss}NMR analyses.

4 Conclusions

The study explored and gave insight into the influence of flue gas on two coal samples and how their respective chemical structural properties respond to a 90-day saturation at 60°C and 9.0 MPa. Several advanced characterisation techniques were applied to probe this behaviour by sample characterisation before and after the occurrence, and the derived conclusions are outlined as follows:

1 The long-term flue gas saturation weakened most functional groups, particularly the aliphatic –OH, C–O, C–C, and the out-of-plane aromatic C–H groups. This was revealed through the UATR-FTIR.

2 The long-term flue gas saturation increased the oxygen-containing functionalities, including the aliphatic carbons bonded to oxygen, f_{al}^{O}, which saw an increase of 42% for the inertinite-rich coal ERL, and 22% for the vitrinite-rich coal SKL.

3 The crystalline diameter and inter-layer spacing were the most affected XRD derived structural properties, such that the crystalline diameter for medium-rank ERL increased by 37.5% with a corresponding increase of 17.3% for high-rank SKL. The relative inter-layer comparison saw a respective decrease of 15% and 22.8% for ERL and SKL.

4 The complex effects of the induced long-term flue gas saturation did not alter the coals' surface morphology; however, there was enough evidence of mineralisation as a result of emerging minerals, including apatite, gypsum, kaolinite, and quartz.

5 Study limitations and proposed future work

Although the study was successful in expanding on the limited fundamental knowledge of direct flue gas injection in unmineable coal seams under in-situ conditions, and its long-term effect on the physicochemical properties of coal, there are some questions that emerged during course of the study period which may assist in expanding the knowledge associated with this study. As a result, the following future research areas are recommended to address some of these questions and limitations:

- An actual industrial flue gas from a coal-fired power plant contains more other components than the ones comprised in the currently studied flue gas including CO, H_2, CH_4, and water vapour H_2O – all in percentage levels; therefore, a flue gas with a bigger spectrum should be synthesised and its sorption properties on different types of coals be investigated, together with the effect this has on the physicochemical properties of the coals.
- The physical and chemical properties of the coals were probed after a maximum of 2,232-hour period of flue gas exposure. This period was satisfactory to detect and observe some of the physicochemical structural changes. It could be more inventive if this period is extended to a minimum of 12 months, this may possibly reveal further flue gas-coal interaction behaviour during sequestration.

References

Ali, M., Jha, N.K., Pal, N., Keshavarz, A., Hoteit, H. and Sarmadivaleh, M. (2022) 'Recent advances in carbon dioxide geological storage, experimental procedures, influencing parameters, and future outlook', *Earth-Science Reviews*, Vol. 225, p.103895, https://doi.org/10.1016/j.earscirev.2021.103895.

Baysal, M., Yürüm, A., Yıldız, B. and Yürüm, Y. (2016) 'Structure of some western Anatolia coals investigated by FTIR, Raman, ^{13}C solid state NMR spectroscopy and X-ray diffraction', *International Journal of Coal Geology*, Vol. 163, pp.166–176, https://doi.org/10.1016/j.coal.2016.07.009.

Chen, R., Zhang, Y., Hu, K., Tu, G. and Dou, T. (2023) 'Changes in physicochemical properties of coal and their mechanism due to supercritical CO_2–H_2O treatment', *Minerals*, Vol. 13, No. 10, p.1262, https://doi.org/10.3390/min13101262.

Cheng, Y., Jiang, H., Zhang, X., Cui, J., Song, C. and Li, X. (2017) 'Effects of coal rank on physicochemical properties of coal and on methane adsorption', *International Journal of Coal Science & Technology*, Vol. 4, No. 2, pp.129–146, https://doi.org/10.1007/s40789-017-0161-6.

Das, D., Agarwal, T. and Biswal, A.K. (2023) 'A review on different methods of CO_2 capture, separation and utilization', *Brazilian Journal of Chemical Engineering*, https://doi.org/10.1007/s43153-023-00378-z.

Du, Y., Sang, S., Wang, W., Liu, S., Wang, T. and Fang, H. (2018) 'Experimental study of the reactions of supercritical CO_2 and minerals in high-rank coal under formation conditions', *Energy & Fuels*, Vol. 32, No. 2, pp.1115–1125, https://doi.org/10.1021/acs.energyfuels.7b02650.

Durucan, S. and Shi, J-Q. (2009) 'Improving the CO_2 well injectivity and enhanced coalbed methane production performance in coal seams', *International Journal of Coal Geology*, Vol. 77, Nos. 1–2, pp.214–221, https://doi.org/10.1016/j.coal.2008.09.012.

Huo, B., Jing, X., Fan, C. and Han, Y. (2019) 'Numerical investigation of flue gas injection enhanced underground coal seam gas drainage', *Energy Science & Engineering*, Vol. 7, No. 6, pp.3204–3219, https://doi.org/10.1002/ese3.491.

Li, X., Zeng, F.G., Wang, W., Dong, K. and Cheng, L.Y. (2015) 'FTIR characterization of structural evolution in low-middle rank coals', *Journal of China Coal Society*, Vol. 40, No. 12, pp.2900–2908.

Liang, Y., Yang, Y., Guo, S., Tian, F. and Wang, S. (2023) 'Combustion mechanism and control approaches of underground coal fires: a review', *International Journal of Coal Science & Technology*, Vol. 10, No. 1, p.24, https://doi.org/10.1007/s40789-023-00581-w.

Lukhele, K.D., Premlall, K., Shongwe, M., Mabuza, M. and Daramola, M.O. (2017) 'Effect of SO_2 co-feeding on CO_2 adsorption capacity of South African coals during CO_2 sequestration', *Petroleum and Coal*, Vol. 59, No. 2, pp.177–186.

Mabuza, M. and Premlall, K. (2023) 'Alterations in the textural structural properties of coals exposed to flue gas for long-term carbon sequestration', *Carbon Capture Science & Technology*, Vol. 7, p.100115, https://doi.org/10.1016/j.ccst.2023.100115.

Mabuza, M., Premlall, K., Onyango, M. and Daramola, M.O. (2018) 'Low-high temperature flue gas direct injection in South African bituminous and anthracite coals: sorption capacity assessment', *Current Science*, Vol. 115, No. 4, pp.682–691, https://www.jstor.org/stable/26978277.

Mastalerz, M., Solano-Acosta, W., Schimmelmann, A. and Drobniak, A. (2009) 'Effects of coal storage in air on physical and chemical properties of coal and on gas adsorption', *International Journal of Coal Geology*, Vol. 79, No. 4, pp.167–174, https://doi.org/10.1016/j.coal.2009.07.001.

Mazumder, S., van Hemert, P., Busch, A., Wolf, K-H.A.A. and Tejera-Cuesta, P. (2006) 'Flue gas and pure CO_2 sorption properties of coal: a comparative study', *International Journal of Coal Geology*, Vol. 67, No. 4, pp.267–279, https://doi.org/10.1016/j.coal.2005.12.001.

Mazumder, S., Wolf, K.H.A.A., van Hemert, P. and Busch, A. (2008) 'Laboratory experiments on environmental friendly means to improve coalbed methane production by carbon dioxide/flue gas injection', *Transport in Porous Media*, Vol. 75, No. 1, pp.63–92, https://doi.org/10.1007/s11242-008-9222-z.

Merey, S. (2022) 'CO_2 sequestration potential in the near-future depleted CO_2 reservoir: Dodan CO_2 field, Turkey', *International Journal of Oil, Gas and Coal Technology*, Vol. 29, No. 1, p.1, https://doi.org/10.1504/IJOGCT.2022.119332.

Pinetown, K.L., Ward, C.R. and van der Westhuizen, W.A. (2007) 'Quantitative evaluation of minerals in coal deposits in the Witbank and Highveld Coalfields, and the potential impact on acid mine drainage', *International Journal of Coal Geology*, Vol. 70, Nos. 1–3, pp.166–183, https://doi.org/10.1016/j.coal.2006.02.013.

Premlall, K., Mabuza, M. and Potgieter, J. (2019) 'Design, construction and performance reliability verification evaluation of a high pressure volumetric sorption system for CO_2 sorption in South African coals', *Petroleum and Coal*, Vol. 61, No. 4, pp.813–835.

Qin, S., Wang, J., Zhao, C. and Zhang, S. (2010) 'Long-term, low temperature simulation of early diagenetic alterations of organic matter: a FTIR study', *Energy Exploration & Exploitation*, Vol. 28, No. 5, pp.365–376, https://doi.org/10.1260/0144-5987.28.5.365.

Raza, A., Gholami, R., Rezaee, R., Rasouli, V. and Rabiei, M. (2019) 'Significant aspects of carbon capture and storage – a review', *Petroleum*, Vol. 5, No. 4, pp.335–340, https://doi.org/10.1016/j.petlm.2018.12.007.

Reddy, K.J., John, S., Weber, H., Argyle, M.D., Bhattacharyya, P., Taylor, D.T., Christensen, M., Foulke, T. and Fahlsing, P. (2011) 'Simultaneous capture and mineralization of coal combustion flue gas carbon dioxide (CO_2)', *Energy Procedia*, Vol. 4, pp.1574–1583, https://doi.org/10.1016/j.egypro.2011.02.027.

Salmachi, A., Zeinijahromi, A., Algarni, M.S., Abahussain, N.A., Alqahtani, S.A., Badalyan, A., Rezaee, M. and Rajabi, M. (2023) 'Experimental study of the impact of CO_2 injection on the pore structure of coal: a case study from the Bowen Basin, Australia', *International Journal of Coal Geology*, Vol. 275, p.104314, https://doi.org/10.1016/j.coal.2023.104314.

Schaeperkoetter, J.C., Connolly, M.J., Buck, Z.N., Taub, H., Kaiser, H. and Wexler, C. (2019) 'Adsorption-induced expansion of graphene oxide frameworks: observation by in situ neutron diffraction', *ACS Omega*, Vol. 4, No. 20, pp.18668–18676, https://doi.org/10.1021/acsomega.9b02589.

Shao, P., Wang, A. and Wang, W. (2019) 'Effect of chemical structure of lignite and high-volatile bituminous coal on the generation of biogenic coalbed methane', *Fuel*, Vol. 245, pp.212–225, https://doi.org/10.1016/j.fuel.2019.02.061.

Syed, A., Durucan, S., Shi, J-Q. and Korre, A. (2013) 'Flue gas injection for CO_2 storage and enhanced coalbed methane recovery: mixed gas sorption and swelling characteristics of coals', *Energy Procedia*, Vol. 37, pp.6738–6745, https://doi.org/10.1016/j.egypro.2013.06.607.

Talapatra, A. (2020) 'A study on the carbon dioxide injection into coal seam aiming at enhancing coal bed methane (ECBM) recovery', *Journal of Petroleum Exploration and Production Technology*, Vol. 10, No. 5, pp.1965–1981, https://doi.org/10.1007/s13202-020-00847-y.

Tcvetkov, P., Cherepovitsyn, A. and Fedoseev, S. (2019) 'Public perception of carbon capture and storage: a state-of-the-art overview', *Heliyon*, Vol. 5, No. 12, p.e02845, https://doi.org/10.1016/j.heliyon.2019.e02845.

Wang, H., Yang, R., Cai, X., Xu, Y., Li, D., Fu, X. and Zhang, D. (2023) 'Long-term supercritical CO_2 exposure dependence of physicochemical properties and CH_4 adsorbability of moisture-equilibrated coal matrices', *Energy Sources, Part A: Recovery, Utilization, and Environmental Effects*, Vol. 45, No. 3, pp.6730–6743, https://doi.org/10.1080/15567036.2023.2216158.

Wu, D. and Zhang, W. (2019) 'Evolution mechanism of macromolecular structure in coal during heat treatment: based on FTIR and XRD in situ analysis techniques', *Journal of Spectroscopy*, pp.1–18, https://doi.org/10.1155/2019/5037836.

Xing, W., Liu, Y. and Zhang, W. (2020) 'Adsorption characteristics of $CO_2/CH_4/N_2$ ternary mixtures on anthracite from 293.15 to 353.15 K and pressures up to 7 MPa', *ACS Omega*, Vol. 5, No. 19, pp.11138–11146, https://doi.org/10.1021/acsomega.0c01083.

Xu, H., Sang, S., Yang, J. and Liu, H. (2021) 'CO_2 storage capacity of anthracite coal in deep burial depth conditions and its potential uncertainty analysis: a case study of the No. 3 coal seam in the Zhengzhuang Block in Qinshui Basin, China', *Geosciences Journal*, Vol. 25, No. 5, pp.715–729, https://doi.org/10.1007/s12303-020-0058-z.

Xu, L., Li, Q., Myers, M., Chen, Q. and Li, X. (2019) 'Application of nuclear magnetic resonance technology to carbon capture, utilization and storage: a review', *Journal of Rock Mechanics and Geotechnical Engineering*, Vol. 11, No. 4, pp.892–908, https://doi.org/10.1016/j.jrmge.2019.01.003

Yu, H., Jing, R., Wang, P., Chen, L. and Yang, Y. (2014) 'Preferential adsorption behaviour of CH_4 and CO_2 on high-rank coal from Qinshui Basin, China', *International Journal of Mining Science and Technology*, Vol. 24, No. 4, pp.491–497, https://doi.org/10.1016/j.ijmst.2014.05.012.

Zhang, G., Ranjith, P.G., Li, Z., Gao, M. and Ma, Z. (2021a) 'Long-term effects of CO_2-water-coal interactions on structural and mechanical changes of bituminous coal', *Journal of Petroleum Science and Engineering*, Vol. 207, p.109093, https://doi.org/10.1016/j.petrol.2021.109093.

Zhang, H., Hu, Z., Xu, Y., Fu, X., Li, W. and Zhang, D. (2021b) 'Impacts of long-term exposure to supercritical carbon dioxide on physicochemical properties and adsorption and desorption capabilities of moisture-equilibrated coals', *Energy & Fuels*, Vol. 35, No. 15, pp.12270–12287, https://doi.org/10.1021/acs.energyfuels.1c01152.

Zhang, Q. (2008) 'Adsorption mechanism of different coal ranks under variable temperature and pressure conditions', *Journal of China University of Mining and Technology*, Vol. 18, No. 3, pp.395–400, https://doi.org/10.1016/S1006-1266(08)60083-8.

Zheng, Y., Li, Q., Zhang, G., Zhao, Y., Zhu, P., Ma, X. and Liu, X. (2020) 'Effect of multi-component gases competitive adsorption on coal spontaneous combustion characteristics under goaf conditions', *Fuel Processing Technology*, Vol. 208, p.106510, https://doi.org/10.1016/j.fuproc.2020.106510.

Zhou, L., Zhou, X., Fan, C., Bai, G., Yang, L. and Wang, Y. (2023) 'Modelling of flue gas injection promoted coal seam gas extraction incorporating heat-fluid-solid interactions', *Energy*, Vol. 268, p.126664, https://doi.org/10.1016/j.energy.2023.126664.